THE ASTROPHYSICAL JOURNAL, 403:412–425, 1993 January 20

THE DISTANT FUTURE OF SOLAR ACTIVITY: A CASE STUDY OF β HYDRI. III. TRANSITION REGION, CORONA, AND STELLAR WIND[1]

D. DRAVINS,[2] P. LINDE,[2] T. R. AYRES,[3] J. L. LINSKY,[4,5] B. MONSIGNORI-FOSSI,[6] T. SIMON,[7] AND F. WALLINDER[2]
Received 1992 January 28; accepted 1992 July 23

ABSTRACT

The secular decay of solar-type activity with age is studied through a detailed comparison of the present Sun (G2 V) with the very old (9–10 Gyr) solar-type star β Hyi (G2 IV), taken as a proxy of the future Sun. Analyses of successive atmospheric layers are made, and this Paper III in the series treats the outermost parts. The far-UV emission lines from the transition zone are among the faintest so far seen in any solar-type star. The significance of the deduced fluxes for the weak and marginally detected lines is tested through two independent reductions of *IUE* data. The coronal soft X-ray spectrum was measured through different filters on *EXOSAT* and compared to simulated X-ray observations of the Sun seen as a star. The flux from β Hyi is weaker than that from the solar corona and has a different spectrum. The complex filter transmission functions preclude a unique determination of the coronal temperature: an emission measure analysis based on an isothermal plasma emissivity model yields *either* $\simeq 5 \times 10^5$ or 4×10^6 K. A corresponding analysis for the Sun "observed" by *EXOSAT* gives 3×10^6 K. The "cool" solution for β Hyi might be physically stable due to a local minimum in the coronal radiative loss function. It is conjectured that this could be an intermediate evolutionary step to losing an observable corona altogether, as is the case in more evolved cool giants. If the "cool" coronal solution is appropriate, it could imply that a thermally driven stellar wind can no longer be supported, removing the mechanism for further rotational braking of the star through a magnetic stellar wind.

Subject headings: stars: coronae — stars: individual (β Hydri) — stars: mass-loss — Sun: activity — Sun: corona — ultraviolet: stars

1. EVOLUTION OF THE OUTERMOST ATMOSPHERE

The present series of papers pursues a detailed examination of the very old solar-type star β Hyi (HR 98 = HD 2151; G2 IV) as a likely proxy for the future Sun. The aim is to find a probable scenario for solar activity in the distant future, when the Sun is twice its present age, and has started to evolve off the main sequence. The basic stellar parameters and evolutionary stage for β Hyi were examined in Paper I (Dravins et al. 1993a), where it was found to be a fully normal single star, of age 9–10 Gyr, originating from nearly the same zero-age main-sequence position as the Sun. Paper II (Dravins et al. 1993b) examined chromospheric activity indicators and their time variability. The chromospheric emission fluxes were found to be about half the solar values, and a monitoring of their time variability suggested a feeble but regular activity cycle somewhat longer than the solar one: of apparent period between 15 and 18 yr. Paper III concludes the series with an analysis of the transition zone, corona, and stellar wind.

Coronal activity and transition region emission seem to be closely connected to stellar magnetic fields. They are very pronounced in young stars, but decrease rapidly with stellar age. Among all spectral types, solar-type stars show the strongest age evolution of coronal X-ray emission. Thus, in very old solar-type stars one could hope to identify some signatures of the "basal" (nonmagnetic) atmosphere, provided the magnetic fields have then largely decayed. However, old stars are difficult to study, both because of their generally much lower activity levels, and the difficulty of age determination. Our target β Hyi is one of only rather few old stars which are both bright enough to permit far-ultraviolet and X-ray studies, while at the same time having a well-understood evolutionary status.

This paper is organized as follows: § 2 describes the spectrum from the transition region; § 3 observations and modeling of the coronal soft X-ray flux; § 4 the implications for a possible stellar wind, while § 5 concludes the paper with an outlook for possible other case studies.

2. THE TRANSITION REGION

2.1. *Far-Ultraviolet Spectra in Solar-Type Stars*

A wide variety of resonance and subordinate lines from abundant atoms and ions which form in the outer layers of the stellar chromosphere and subcoronal "transition region" (10^4–10^5 K) are observable in the short-wavelength ultraviolet. Usually, hydrogen Lyα is the brightest of these: it is optically thick, and forms not only in the high chromosphere but also over a broad range of temperatures which might possibly include even coronal structures (e.g., Bonnet et al. 1980). The next strongest emissions are the resonance lines of C II (near 133.5 nm) and C IV (near 154.9 nm): they form at a few times 10^4 and 1×10^5 K, respectively.

The *International Ultraviolet Explorer* (*IUE*) satellite is capable of recording low- and high-dispersion spectra down to 115 nm. Previous studies (e.g. Ayres, Marstad, & Linsky 1981b) have demonstrated that solar-type stars exhibit a diverse range of emission levels in their transition-region spectra, presumably related to differing degrees of surface magnetic activity. Typically, young fast-rotating stars show the

[1] Based on observations (a) by the *International Ultraviolet Explorer*, and (b) by the *EXOSAT* satellite of the European Space Agency.

[2] Lund Observatory, Box 43, S-22100 Lund, Sweden.
[3] Center for Astrophysics and Space Astronomy, University of Colorado, Campus Box 391, Boulder, CO 80309.
[4] Joint Institute for Laboratory Astrophysics, University of Colorado, Campus Box 440, Boulder, CO 80309.
[5] Staff member, Quantum Physics Division, National Institute of Standards and Technology.
[6] Osservatorio Astrofisico di Arcetri, Largo Enrico Fermi 5, I-50125 Florence, Italy.
[7] Institute for Astronomy, University of Hawaii, 2680 Woodlawn Drive, Honolulu, HI 96822.

highest surface flux densities of C IV 154.9 nm, while middle-aged slowly rotating stars like the Sun and its nearby "twin" α Cen A tend to fall at the bottoms of the flux distributions. In order to explore the early post–main-sequence fate of a solar-like transition region, we have studied β Hyi with the *IUE* in its low-dispersion mode to measure line fluxes (with resolution $\simeq 0.5$ nm = 5 Å) and in its high-dispersion mode to record line profiles (resolution $\simeq 0.01$ nm).

2.2. IUE *Observations*

2.2.1. β *Hydri*

Far-ultraviolet spectra of β Hyi have been obtained under a number of observing programs, and Table 1 catalogs the exposures available in the *IUE* archive as of this writing. The faintness of the emissions from the transition region necessitates long integration times, and of special note are our observations of 1982 February 12/13. Three consecutive *IUE* shifts were devoted to β Hyi, resulting in low-dispersion spectra of 20 minutes integration time (SWP 16324), 25+160 minutes (double exposure in large aperture: SWP 16323a and SWP 16323b), and one 16 hr high-dispersion exposure (SWP 16325; conducted over consecutive *VILSPA* and US1 shifts). The stellar flux changes rapidly with wavelength, and widely different exposure times are required to map out the faintest portions (125–160 nm), as well as the relatively bright, largely photospheric continuum in the 175–195 nm region.

2.2.2. *Comparison Stars*

Additional G2 stars were selected to compare with the far-ultraviolet spectrum of β Hyi. These in particular included α Cen A (G2 V), which is quite comparable in activity level to the quiet Sun (e.g., Ayres, Simon, & Linsky 1982)—and presumably also to the main-sequence predecessor of β Hyi. In addition, the spectrum of the active bright giant β Dra (G2 Ib–II) will be displayed below, indicating which spectral lines that are present in high-activity stars.

2.3. *Photometric Reduction and Spectrum Extraction*

2.3.1. *Reduction of Low-Dispersion Data*

Two independent reductions of these *IUE* observations were made, using different spectrum extraction procedures. One was undertaken in Lund (D. D. & P. L.), starting with a geometric and photometric reprocessing of the raw spectral images, using methods analogous to those used in the Mg II *h* and *k* line analysis, as described in the Appendix of Paper II. The other was done in Boulder (T.R.A.), by photometrically linearizing the raw images using an intensity transfer function based on the 1985 recalibration of the SWP camera; identifying and removing pointlike cosmic-ray hits and other transient defects using an automated numerical filter; deriving, and subtracting, an off-spectrum background by spatially filtering and heavily smoothing the fluxes in two bands above and below the spectral swath; and extracting the spectrum using an "optimal" weighted slit, like that described by Kinney, Bohlin, & Neill (1991), based on the local cross-dispersion profile of the spectral trace and a "noise model" that assigns a photometric uncertainty to each pixel flux according to its intensity. The optimal extraction explicitly accounts for spatially extended spectral traces like the double exposure of β Hyi (SWP 16323a & b) and is designed to track the spatial "undulations" of the spectrum which result from shears in the camera's fiber-optic coupler.

TABLE 1

IUE SHORT-WAVELENGTH EXPOSURES OF BETA HYDRI

IUE Image Number (1)	Dispersion (2)	Aperture (3)	Exposure Time (minutes) (4)	Date (5)
SWP 1689	L	S	20	1978 Jun 2
SWP 4760	L	T + S	10 + 10	1979 Mar 26
SWP 6128	L	L + S	17 + 3	1979 Aug 9
SWP 7307	L	L + S	80 + 10	1979 Dec 3
SWP 7429	L	L	12	1979 Dec 18
SWP 7430	L	L	210	1979 Dec 18
SWP 16323a + b	L	D	25 + 160	1982 Feb 12
SWP 16324	L	L	20	1982 Feb 12
SWP 16325	H	L	938	1982 Feb 13
SWP 38286	L	L	12	1990 Mar 2

NOTES.—Col. (2): L = low, H = high dispersion. Col. (3): S = small, L = large aperture, T = trailed, D = double-exposure in large aperture.

The spectral features in the far-ultraviolet are faint, and the availability of two independent spectrum extractions (each superior to standard *IUE* software) permits a more credible discussion of the reality of the less certain of these. Further, a comparison of the flux values deduced by independent methods gives a first hint of the probable level of systematic errors generally remaining in such *IUE* data. Such errors might originate from, for example, the difficulties of relative flux calibration when no measurable stellar continuum is available nearby, while the use of the instrumental calibration becomes uncertain if the spacecraft pointing would not always keep the target star properly centered.

2.3.2. *The Appearance of IUE Spectrograms*

For display purposes we merged together a number of the photometrically corrected spectral images of β Hyi and its comparison stars. These images show the reality (or otherwise) of detected (or previously claimed) faint spectral features, illustrate the character of the remaining noise, and contrast the transition region spectra among G stars of widely different activity levels. Such co-added images are shown here for the Lund reduction procedure (Fig. 1). To show emission features throughout the spectrum, exposures of different length are combined, and the smooth photospheric continuum rise toward longer wavelengths was fitted to a spline function, and then subtracted. For clarity, the spectrograms are stretched a factor 2 perpendicular to the dispersion. The spatial "undulations" of the spectrum are apparent: a reliable extraction requires a weighted slit that can accurately track the centroid of the spectral trace.

The β Hyi spectrogram depicted in Figure 1 is a combination of SWP 16324 (20 minutes exposure) around Lyα, SWP 16323b (160 minutes) between 123 and 169 nm, and again SWP 16324 out to 190 nm. The Lyα feature is elongated along the axis of the large spectrometer aperture owing to superposed geocoronal emission, comparable in strength to the stellar Lyα. Despite the very deep exposure, only weak emission features are seen: the transition region spectrum of β Hyi appears to be one of the faintest so far observed in any solar-type star.

α Cen A also is a low-activity star, reminiscent of the Sun at its activity minimum. The spectrogram in Figure 1 is composed by SWP 28486 (3 minutes) around Lyα, SWP 28487 (20 minutes) between 123 and 169 nm, and SWP 28486 out to 190 nm. The difference in apparent magnitude makes these

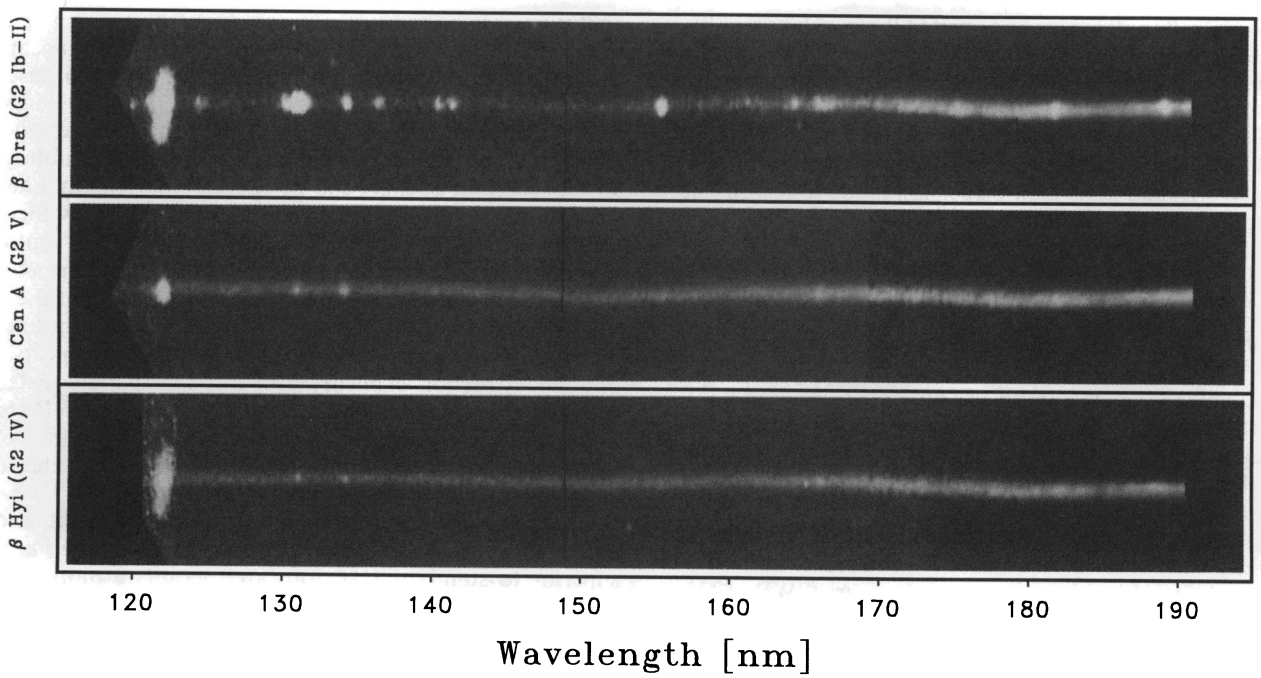

FIG. 1.—Photometrically processed images from the *IUE* low-dispersion camera illustrate the great range of transition-zone emission in G2 stars. Exposures of different length are combined, and the photospheric continuum subtracted. The emission features in β Hyi are among the faintest observed from the transition region of any solar-type star. α Cen A is reminiscent of the Sun at its activity minimum, while the active bright giant β Dra displays a rich emission-line spectrum. These data were processed with the Lund method.

images very similar in exposure level to those of β Hyi. The Lyα line, however, now is almost fully stellar, with only a small geocoronal contamination. Beta Dra is an unusually active bright giant, and its SWP 15292 image illustrates a rich emission-line spectrum, even at a much shorter exposure (30 minutes) than for β Hyi, which is of identical apparent magnitude. Its spectrum serves in particular to illustrate the wavelength positions of several emission lines that are very faint or absent in β Hyi. The Lyα feature in β Dra is almost wholly geocoronal, owing to the severe interstellar attenuation of the intrinsic emission from this distant star.

2.3.3. *Spectrum Extraction and Calibration: The Lund Procedure*

Because of a rapid change with wavelength of the stellar flux, and the limited dynamic range of the *IUE* detector, data from different exposures were combined: SWP 16324 in the Lyα region; SWP 16323b in the interval 122–169 nm, SWP 16323a for 160–186 nm, and SWP 16324 for 160–190 nm.

The Lyα region is contaminated by geocoronal emission, and to recover the stellar profile, the geocoronal (plus ordinary) background was subtracted, as measured on both sides of the spectrum in SWP 16324. For β Hyi, this correction amounts to about one-half of the gross signal, i.e., comparable to the remaining stellar part, and the recovered stellar Lyα flux should be correct to within some 20% or so.

To place the extracted spectra on an absolute flux scale, the flux calibration in the *IUE* observatory standard software (IUESIPS) was used, following an additional correction for instrumental stray light. For cool stars, the "continuum" seen below $\simeq$160 nm is largely stray light from longer wavelengths. A simple correction was made, by measuring the exposure level *shortward* of Lyα (where *IUE* has essentially no sensitivity, and the true measured stellar flux must be almost zero), and subtracting that value, assumed constant throughout the spectrum. Already this simple correction is sufficient to eliminate the fortuitous "bumps" (i.e., spurious maxima in the apparent photospheric continuum), otherwise commonly seen in *IUE* spectra. These reflect the corresponding "bumps" in the sensitivity function, rendered visible by the presence of stray light. For example, such a "bump" around 155 nm is prominent in the β Hyi data used for the ultraviolet calibration of the *Hubble Space Telescope* (Bohlin et al. 1990).

To compare to the fluxes at the surface of the other G2 stars, the spectra were normalized in the longward 170–180 nm part, where the photospheric continuum begins to emerge. At the effective temperature of β Hyi, α Cen A, and the Sun, the bolometric surface flux is 6.3×10^7 W m^{-2}.

A similar processing was applied to spectral images of α Cen A, but no correction for geocoronal Lyα was made (the apparent brightness of α Cen A is much greater than that of β Hyi, and the relative contamination an order of magnitude smaller).

The calibrated spectra extracted with the Lund procedure were finally measured interactively, and the resulting line fluxes are in Table 2.

2.3.4. *Spectrum Extraction and Calibration: The Boulder Procedure*

For each of the stars, the extracted large-aperture spectra (aside from the trailed exposure SWP 4760 for β Hyi) were combined together, weighting each flux f_λ by the inverse of its assigned variance ($w_\lambda = 1/\sigma_\lambda^2$). The co-added spectra were then measured using a semiautonomous line-finding and fitting algorithm that fits a smooth continuum and models the significant emissions above it using a Bevington-type multiple-Gaussian procedure.

The results are shown in Figure 2 and Table 2. Since the Lyα feature of β Hyi is affected by geocoronal contamination, its profile and flux was determined from the four large-aperture exposures of 20 minutes or less; for which the contrast between the stellar and geocoronal features appears greatest. The optimal fitting of the Lyα feature naturally suppresses the con-

TABLE 2

EMISSION-LINE FLUXES FROM THE TRANSITION REGIONS IN β HYI, α CEN A, AND THE SUN

Emission Line (nm)	β Hyi (W m^{-2})	β Hyi ($10^7 f_L/f_{bol}$)	α Cen A ($10^7 f_L/f_{bol}$)	Sun (min – max) ($10^7 f_L/f_{bol}$)	Average, Variability
H I 121.6	98 ± 20 (193 ± 3)	16 (31.0)	28 (15.2)	30 –110[1]	33[2], 51%
N V 124.0	<1 (<0.6; 3σ)	<0.2 (<0.1)	<0.2 (0.24)	0.06–0.14[3]	
O I 130.5	6.0 ± 1 (5.5 ± 0.2)	1.0 (0.88)	1.1 (0.94)	0.7 –1.6[3]	0.7[2], 25%
C II 133.5	5.1 ± 1 (4.0 ± 0.2)	0.8 (0.63)	1.3 (0.96)	0.8 –2.4[3]	1.0[2], 25%
Si IV 140.0	<1 (2.9 ± 0.3)	<0.2 (0.47)	<0.2 (0.41)	0.4 –1.1[3]	0.6[2], 33%
C IV 154.8	2.8: ± 2 (5.1 ± 0.5)	0.4 (0.82)	0.4 (0.56)	0.9 –2.1[3]	1.1[2], 44%
C I 165.7	5.9 ± 2 (6.9 ± 0.7)	0.9 (1.1)	1.0 (0.9)		0.8[4], 1.6:[2], 28%
Si II 181.7	9.7 ± 2 (30:[a])	1.5 (5:)	1.9 (3:[a])	3.1 –3.5[3]	

NOTE.—Two independent sets of values are given, as obtained from two different schemes of *IUE* data processing made in Lund (open text), and in Boulder (in parentheses). The β Hyi and α Cen A data are directly comparable, as they have been extracted from *IUE* spectra exposed to nearly the same level, and processed in an identical fashion. The solar data indicate typical amplitudes during an activity cycle. Fluxes are given at the stellar surface in (W m^{-2}) = (10^3 ergs s^{-1} cm^{-2}) and as the fraction of the bolometric flux f_{bol}. The solar data are from (1) Lean 1987; (2) average over 1982.0–1986.0 by Bennett (1987); (3) Ayres et al. 1981; (4) Ayres & Linsky 1980. The solar variability (%) is indicated by the mean flux last 50 days of 1985 (near minimum activity) divided by first 50 days of 1982 (near maximum; Bennett 1987). No corrections of interstellar absorption have been made.

[a] λ180.0 & 181.7; uncertain flux due to low contrast against bright photospheric continuum.

tribution of the spatially extended geocoronal feature, although the correction may not be complete. The spectrum of α Cen A (otherwise based on SWP 28486 and SWP 28487) was similarly restricted in the vicinity of Lyα (SWP 13886 only).

The Boulder-reduced spectra were corrected for scattered light in the same way as the Lund-processed ones, and placed on an absolute scale by reference to a calibration based on the DA white dwarf G191-B2B (very similar to the method used in the IUESIPS). The ordinate in Figure 2 is calibrated flux at Earth, with a scaling between the diagrams that approximates the relative appearance in f_λ/f_{bol}. The crosses mark portions which are affected by an incompletely removed fiducial reseau.

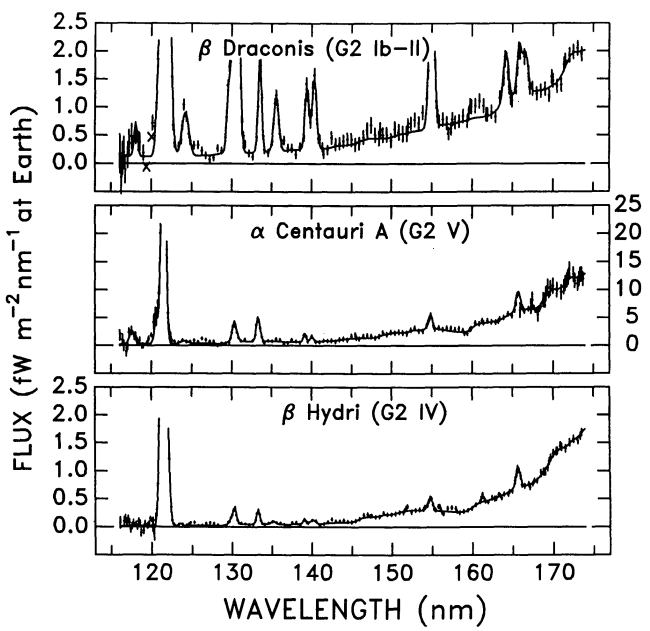

FIG. 2.—The far-ultraviolet spectrum of β Hyi, compared to that of other G2 stars. The derived continuum traces and multiple-Gaussian fits to a key group of emission lines are overlaid (*solid curve*) onto co-added low-dispersion SWP spectra (*dots*). The spectrum of the active bright giant β Dra indicates which spectral lines that are present in high-activity stars, but are absent in β Hyi. One unit of femtowatt per square meter per nanometer equals 10^{-13} ergs cm^{-2} s^{-1} Å^{-1}. These data were processed with the Boulder method.

2.4. *Spectral Properties*

The diagnostic properties of different transition region lines are reviewed, e.g., by Haisch et al. (1990). The O I 130.5 nm can be strong in noncoronal stars because it is pumped by the Lyβ line. While it thus indicates the *presence* of a chromosphere, it is a poor diagnostic of chromospheric conditions, because it is not collisionally excited. The C II 133.5 nm doublet is often strong in solar spectra. Although it originates at the modest temperatures of 10,000–25,000 K, it behaves much as a transition-region line. C I 165.7 nm is a chromospheric multiplet, identified as a pumping transition (along with Lyβ and O I). Among all potential diagnostics, C IV 154.8 and Si IV 139.4 and 140.2 nm are the most representative of transition region emission, forming around 10^5 K; e.g., Jordan et al. (1987).

The spectrum of α Cen A is similar to the Sun at activity minimum (e.g., Haisch & Basri 1985; Cappelli et al. 1989), and also to β Hyi. While emission lines from neutral species (O I 130.5 and C I 165.7 nm) are very similar, lines from singly ionized species appear to be somewhat weaker in β Hyi (C II 133.5, Si II 181.7). The important C IV and Si IV emissions appear to be comparable in the two stars.

The *solar* UV spectrum, at a spectral resolution similar to IUE data, is discussed by some authors. Cappelli et al. (1989) compare stellar data to spectrally smoothed SKYLAB spectra of various solar surface features, while Haisch & Basri (1985) use rocket spectra of disk-integrated flux at epochs of maximum and minimum solar activity to compare with spectra of G0 V–G5 V field stars. Their emissions are typically a factor of 5 stronger than those of β Hyi, further underscoring the weakness of its features. However, as noted by Cappelli et al., the emission fluxes from (nonmagnetic) quiet solar regions are often weaker than those from any low-activity star.

2.4.1. *Different Spectrum Extractions*

For lines from multiply ionized species, there are differences in what was identified in the Boulder, and in the Lund-processed data. While the Si IV feature is a positive detection in the Boulder-processed co-added spectrum of β Hyi (Fig. 2), it was not seen in the Lund-processed spectra (Fig. 1). Previously, *IUE* spectrum extractions performed with automated standard software have suggested the presence also of N V 124.0 nm (Simon & Drake 1989) and, following a reexamination of that

work, its authors confirm their conclusions. However, neither the Boulder nor the Lund extractions were able to find this N v line. Such discrepancies, however, should be viewed as normal in searches for faint spectral features at the very limits of the *IUE* capability. In any case, the transition-region spectrum of β Hyi is among the faintest so far seen in any solar-type star. To decide on the strengths of the fainter lines will not be possible from *IUE*, and one will need greatly improved data, e.g., from the *Hubble Space Telescope*.

2.4.2. *Lyα*

The hydrogen Lyα line is excited mostly by collisions, while Lyβ, Hα, and the Lyman continuum are controlled by the Lyα radiation field (Skumanich & Lites 1986). Lyα is thus primarily a chromospheric diagnostic which, due to the large abundance of hydrogen, is formed high in the chromosphere. The exact formation conditions are model-dependent and may be quite uncertain due to the largely unknown effects of magnetic structures. Thus, Fontenla, Avrett, & Loeser (1990) find the Lyα center to be formed at temperatures between 40,000 and 70,000 K, rather hotter than found in some earlier models.

In cool dwarfs, Lyα is normally the strongest emission line in the short-wavelength ultraviolet, and one of the most important cooling agents for their outer atmospheres. Unfortunately, uncertain corrections for interstellar absorption and geocoronal contamination render Lyα less suited for studies of *absolute* emission properties, but it still is a valuable diagnostic in comparative studies of nearby stars.

The Lyα line seems fainter in β Hyi than in α Cen A, both of which are weaker than in the Sun. However, the exact flux value depends on precisely how the geocoronal emission has been accounted for, and there are two somewhat different values in Table 2. A third reduction has been made for a catalog of Lyα fluxes being prepared by Landsman & Simon (1993), where they obtain $f_{\mathrm{Ly}\alpha}/f_{\mathrm{bol}} = 16.5$ and 16.9×10^{-7}, respectively, from two low-dispersion spectra of β Hyi. These agree with the Lund value in Table 2, but not with the Boulder extraction. Landsman & Simon extracted their fluxes from an IUESIPS line-by-line file, removing a modeled geocoronal background, scaled to the off-spectrum geocoronal flux. Böhm-Vitense & Woods (1983) surveyed Lyα in a number of F and early G stars, finding $f_{\mathrm{Ly}\alpha}/f_{\mathrm{bol}} = 7.1 \times 10^{-7}$ in β Hyi (after reducing for geocoronal effects), the lowest Lyα flux value among their G stars. Parts of these flux differences could be due to the changing instrumental sensitivity (and calibration) during the *IUE* mission.

Any more detailed interpretation of Lyα requires a careful analysis of the effects of interstellar absorption. Although Landsman & Simon (1991) used Lyα emission observed from *IUE* in late-type stars across the sky to conclude that the local interstellar medium is relatively free of neutral hydrogen, local interstellar hydrogen may nevertheless attenuate the flux from even the nearest stars by a factor of 2 (Landsman et al. 1986). Interstellar effects were also discussed by Böhm-Vitense & Woods (1983).

2.5. *The Far-Ultraviolet Spectrum in High Dispersion*

As the centerpiece of our observational effort, we exposed a deep SWP echellogram for 938 minutes, during the low charged-particle radiation period of a VILSPA and US1 shift pair. While the image (SWP 16325) was overexposed in the long-wavelength continuum ($\lambda > 190$ nm), it is essentially blank below about 170 nm except for faint (stellar) Lyα wings extending longward from the overexposed geocoronal features in echelle orders 113 and 114. We have made a detailed examination of the spectral image, e.g., blinking it against similar images of other stars, but the exposure and noise levels do not permit the identification of any other stellar lines shortward of 180 nm. The only useful emission profiles recorded in the otherwise disappointing echellogram are those of Si II around 181 nm, in echelle order 76. A plot of that region, photometrically extracted with the Lund procedure, is depicted in Figure 3. The cores of the two longward Si II lines were overexposed, and the dotted lines show our estimated extrapolation to their true intensities, as deduced from analyzing the original spectral image, and comparing with other overexposures of lines with known strengths.

The Si II lines are formed in the lower transition zone at temperatures around 2×10^4 K (e.g., Brown et al. 1984; Jordan et al. 1987). Unfortunately, the Si II features in and of themselves are not particularly informative: their measured full widths at half-maxima are $\simeq 30$ km s^{-1}, not much in excess of the instrumental broadening of $\simeq 20$–25 km s^{-1}. The widths and relative intensities of lines in the triplet are comparable to those of the well-observed counterparts in the spectrum of the K giant Arcturus (Ayres et al. 1986), but differ from those in the bright G giant β Dra (Brown et al. 1984). However, the lines are exceedingly optically thick and consequently a poor diagnostic for chromospheric Doppler velocities. Ideally, we would have recorded profiles of the density-sensitive Si III] 189.2 and C III] 190.9 nm features, but the bright photospheric continuum longward of 190 nm precludes that possibility. Application of profile diagnostics and density-sensitive line ratios in the case of β Hyi is beyond the grasp of the *IUE* and must await future spectroscopic work with superior instruments.

2.6. *Plasma Models for the Transition Zone Emission*

The surface fluxes of those high-excitation emissions that can be reliably measured in the co-added low-dispersion *IUE* spectrum of β Hyi are quite comparable to those of the Sun at the minimum of its activity cycle. Thus, the distribution of emission-measure $\mathrm{EM} \equiv \int n_e^2\, dz$ (cm^{-5}) with temperature will also be similar to that of the quiet Sun. Anticipating the results of a subsequent section, we find that existing X-ray observations of β Hyi (by *EXOSAT*) admit to two possible coronal configurations: either a "cool" solution with $\log T \simeq 5.7$, or a hot solution with $\log T \simeq 6.6$ K. Unfortunately, the emission

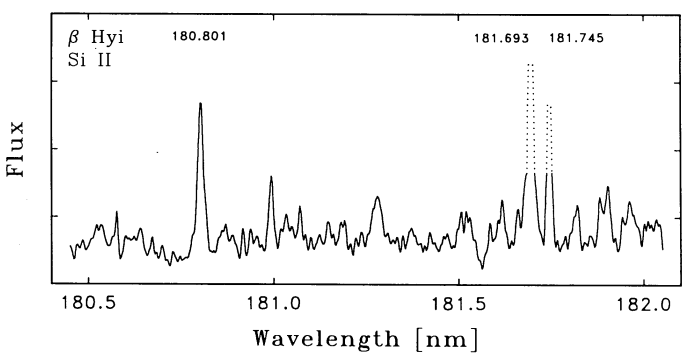

FIG. 3.—The Si II triplet around 181 nm in β Hydri, observed with *IUE* in high dispersion. The two longward Si II lines were overexposed, and the dotted lines show our estimated extrapolation to their true intensities. The widths and relative intensities of lines in the triplet are similar to those of the K giant Arcturus, but differ from those in the bright G giant β Dra.

measure distribution derived from the far-UV lines cannot confirm or exclude either of the coronal solutions because even the hottest diagnostic—N v 124.0 nm, not positively detected in the spectrum of β Hyi—has its maximum abundance at temperatures well below either of the coronal configurations. Nevertheless, if the "cool" solution is appropriate, one has a situation somewhat different from the Sun: the emission measure distribution would continue to decline through the temperature range $\log T > 5.0$, whereas in the Sun and other late-type dwarfs, the EM distribution tends to rise toward coronal temperatures (e.g., Jordan 1991) after reaching a minimum at 10^5 K. The apparent decline in the coronal emission measure, if genuine, could be signaling a fundamental weaking of the coronal layers; the beginning of the process that ultimately leads to the "death" of solar-like coronal activity in old solar-mass K giants like Arcturus (e.g., Ayres, Fleming, & Schmitt 1991). The resolution of the issue will require additional information, e.g., the emission-measure distribution of the intermediate temperature region $5.3 < \log T < 6.0$. Upper limits on the extreme-UV flux exist for 4–80 nm (Ayres et al. 1978), as measured from the *Apollo-Soyuz* EUV grazing incidence telescope. However, these limits are much higher than the flux that could be expected from β Hyi, although the wide field EUV camera onboard *ROSAT* might have the required sensitivity. A further requirement is to determine electron densities, e.g., from line ratios such as the O IV λ140.0 nm multiplet.

2.7. *The Evolution of Stellar Transition Regions*

Despite the relative weakness of the β Hyi transition zone features, the comparisons in Figure 2 and in Table 2 nonetheless demonstrate that its normalized fluxes are not very different from those in α Cen A and the average Sun. This is a somewhat unexpected result, given the common belief that transition region activity subsides as $\simeq 1\,\mathfrak{M}_\odot$ stars evolve away from the main sequence.

Such evidence has been collected by Simon, Herbig, & Boesgaard (1985), who discuss the evolution of various activity indicators with stellar age, noting that the *e*-folding time for high-excitation transition region lines is substantially shorter ($\simeq$1.4 Gyr) than that for lines formed in the low chromosphere ($\simeq$2.6 Gyr). (However, they never discussed stars as old as β Hyi, so these times may not be representative of very old stars.) For 1 $\mathfrak{M}_\odot$ stars, there is approximately one order of magnitude decline in the intensity of the UV emission during their main-sequence lifetimes. These trends are confirmed by flux-flux diagrams (correlating chromospheric and transition region fluxes), which demonstrate how high-excitation lines from hotter regions are the ones to decay most rapidly when stellar activity (as measured in Ca II or Mg II) weakens; e.g., Oranje (1986); Haisch et al. (1990).

Simon & Drake (1989) studied activity parameters for cool subgiants, finding that once these stars have finished their main-sequence life, there seems to be no further major change in their activity levels (as measured by C II and C IV ultraviolet emission), the fluxes remaining comparable to those of the quiet Sun, at least until the stars start their ascent of the red giant branch. If correct, this indicates that stars such as β Hyi do indeed represent the lowest possible level of transition zone activity in solar-type stars, a level which will again increase during the later stellar evolution. While this is consistent with our findings of β Hyi, it is inconsistent with some dynamo models, where a resurgence of activity instead should have occurred due to the deepening convection zone (cf. § 4 in Paper I). The results are also consistent with the suggestion that stellar dynamos are quite inefficient at slow rotation speeds.

3. THE CORONA

Coronal X-ray fluxes are particularly strong among young main-sequence stars but often much weaker in evolved ones. For example, the flux from the slightly evolved solar-type star α Cen A (G2 V) is comparable to the solar one at activity minimum (Golub et al. 1982). However, no X-rays have been found from the more evolved solar-mass star Arcturus (K1 III), even at a surface flux level only 1×10^{-4} that of α Cen A, a 3 σ upper limit set by *ROSAT* measurements in the energy band 0.1–2.4 keV (Ayres et al. 1991). Such examples indicate that coronal activity decays much more steeply with increasing stellar age, than do chromospheric indicators. However, if the coronae of evolved stars are cooler than $\simeq 10^6$ K, the upper limits set by *Einstein* or *ROSAT* are not very meaningful since their instrumental lack of sensitivity to the lowest energy X-rays rapidly lowers the detectability of cooler sources. High-resolution X-ray spectra would clarify many questions, but their general nonavailability at present precludes more detailed studies. For a general introduction to stellar X-ray emission, see Palavicini (1989).

The post–main-sequence evolution of solar-type coronae is even less understood than that of chromospheric activity. Does the coronal activity perhaps fall very rapidly after the star has left the main sequence? While coronae can be seen in some G giants, ordinary single giants later than early K normally do not have measureable X-ray fluxes (Haisch, Schmitt, & Rosso 1991). Is the reason that magnetic flux is no longer generated, or is it connected with the lower photospheric pressure which cannot compress sufficiently strong magnetic fields? Is the remnant corona then representative of the minimal stellar "basal" activity, mainly heated by acoustic waves from the photospheric granulation? However, models of acoustic heating have been unable to explain even very low emission coronae: while acoustically heated atmospheres might produce chromospheric emission lines, they appear incapable of emitting significant amounts of X-ray flux (Stepień & Ulmschneider 1989). Have there perhaps been significant changes in the stellar wind, upsetting the coronal cooling mechanisms? What processes occur in stars that are losing their coronae between the main sequence and the giant stage? Will they first keep the coronae at cooler ("lukewarm") temperatures before losing them altogether? And does a solar-type star still have a corona at the age of β Hyi?

We have studied the corona of β Hyi through *EXOSAT* observations of its soft X-ray flux in different spectral regions. In this section, we describe these observations and their interpretation with models of high-temperature plasmas and further discuss the implications for understanding the mechanisms of coronal heating and their time evolution.

3.1. *EXOSAT Observations*

The corona of β Hyi was observed with the LE1 low-energy X-ray imaging telescope on board ESA's *EXOSAT* satellite, using different filters in front of the CMA (channel multiplier array) detector. Although the filter transmission curves are rather jagged and irregular, observations through successive filters enable a rough estimate of the X-ray spectrum. A general description of this instrument is by de Korte et al. (1981), and Taylor (1985), while the transmission curves of the filters are included in Figure 7 below. A detailed calibration of the

EXOSAT instruments has been made by Paerels et al. (1990). *EXOSAT* was sensitive to a considerably broader wavelength interval (≃0.5–60 nm; 0.02–2.5 keV) than *Einstein* (≃0.3–6 nm; 0.2–4 keV; also comparable to *ROSAT*).

Our observations were made on 1984 September 22. The soft X-ray flux was measured in an exposure of nominally 60 minutes through the "thin" 3000 Lexan filter, in a nominally 92 m exposure through the aluminum + Parylene filter, and an upper limit for harder X-rays could be set in a 154 m exposure through the boron filter. The 3000 Lexan filter is centered on ≃150 eV photon energy, corresponding to ≃8 nm (80 Å). The aluminum + Parylene filter has an effective area comparable to that of the Lexan filter, but is especially sensitive to softer X-rays around 60 eV ≃ 20 nm. The boron filter has dual transmissions, both in soft and in hard X-rays. For early-type stars (with significant ultraviolet flux) there is a risk of the signal being contaminated by UV radiation leaking through the filters. However, for stars as cool as β Hyi, such effects are negligible, and the filter most severely affected by UV leaks (polypropylene) was not used in the present observations.

The *effective* exposure times for the three filters turned out to be 3541, 4089, and 7278 s, respectively. These are shorter than the nominal ones because of dead time due to background events (above certain values of the solar particle radiation, the data are rejected). Estimated photon counts from β Hyi were 61.9 ± 9.9 (source significance 10.3 standard deviations); 39.6 ± 9.2 (5.9 s.d.); and 1.4 ± 7.5 photon events, for the three filters, respectively. From these data, the following count rates result: Lexan $1.75 \pm 0.3 \times 10^{-2}$ s^{-1}; Al/P $9.7 \pm 2 \times 10^{-3}$ s^{-1}, and an upper limit for boron $< 1.4 \times 10^{-3}$ s^{-1}. The upper limit for boron is less stringent than could have been possible, had there not been a command error in pointing the spacecraft, placing β Hyi some 16′ off center in the field of view. The point spread function there is ≃35″ instead of ≃18″ on axis, correspondingly raising the detection limit. The detailed interpretation of the boron data is further made complicated by the energy dependence of the imaging in the telescope and/or through the filters, resulting in a wider point-spread function for the higher energy X-rays (Davelaar & Giommi 1985; Paerels et al. 1990).

The count rates were obtained with the *EXOSAT Observatory* automatic analysis software. The same data were also reprocessed as by Pallavicini et al. (1988), yielding somewhat different count rates. While these differences are small enough not to affect our conclusions below, they do illustrate that there may exist systematic errors in addition to the statistical ones.

The filter effective areas used below are the best estimates of their in-orbit performance. The preflight filter data are reduced to 73% due to a mechanical obscuration of the LE1 telescope by an overopened flap on the adjacent medium-energy instrument (Gottwald 1985) and are further corrected for the transmission of a plasma suppression grid (95%).

3.2. *Simulated X-Ray Observations of the Sun*

A first comparison to make is with the X-ray flux from the solar corona. *Simulated observations* of the Sun seen as a star by *EXOSAT* were made by folding the known solar X-ray spectrum with the transmission curves of the different *EXOSAT* filters. By "placing" the Sun at the distance of β Hyi, a direct comparison to the observed count rates in different *EXOSAT* filters is achieved. Solar far-UV and X-ray fluxes were taken from the compilations by Kreplin et al. (1977), Manson (1977) and Timothy (1977). A number of different solar values were used, in particular those corresponding to "minimum" and "maximum" fluxes. These flux spectra were converted from energy to photon numbers, and suitably multiplied with the effective areas of each *EXOSAT* filter in the energy intervals between 0.02 and 2.5 keV. The Sun was then "placed" at the distance of β Hyi (6.54 pc, assuming negligible interstellar extinction), and a summation of the photon count level inside the passband of each filter was made.

Table 3 shows that the β Hyi flux in the Lexan band is comparable to the solar value but is significantly lower in the Al-Pa region. This comparison does not account for the greater size and luminosity of β Hyi: if one normalizes to stellar surface area and bolometric luminosity, the difference to the Sun is enhanced (bottom line in Table 3). In any case, the differences in count rates between the Sun and β Hyi demonstrate (*a*) that the flux from the corona of β Hyi is markedly lower, and (*b*) that the *shape* of its X-ray spectrum is different from that of the present Sun.

3.3. *Coronal Models for β Hydri and the Sun Seen as a Star*

The different spectral response of the different *EXOSAT* filters permits one to deduce a color temperature for the X-ray emitting plasma (assuming isothermal conditions). For the interpretation of the data, models of synthetic X-ray spectra from optically thin astrophysical plasmas were applied. A number of different models have been developed for this purpose, and we chose those by Landini & Monsignori-Fossi (1984, 1990). Of significant importance is that their calculations extend over a larger wavelength interval and a greater temperature range than most other work. This is required to fully cover the energy range of *EXOSAT* observations of very soft X-rays, and to study UV lines from ions at temperatures lower than 10^6 K.

The emission of an optically thin and low-density plasma is computed for a temperature grid $10^4 < T < 10^8$ K, and for wavelengths between 0.1 and 200 nm (1–2000 Å). The spectrum includes bremsstrahlung, recombination, and line emission. About 1000 emission lines are included, collisionally populated from the ground level, and selected following isoelectronic sequences (from H, He, C, N, O, Ne, Mg, Si, S, Ar, Ca, Fe, and Ni). The continuum emission includes free-free radiation, free-bound radiation from all ions of the mentioned elements, and two-photon emission from hydrogen-like atoms. The model's emissivity versus λ for various temperatures, and the line emissivity for various species can be seen in Landini & Monsignori-Fossi (1984, 1990). Such models have been com-

TABLE 3

EXOSAT SOFT X-RAY FLUXES

	FILTER		
	3000 Lexan	Aluminum/Parylene	Boron
"Minimum Sun"	38	65	1
"Maximum Sun"	90	142	3
Beta Hydri	63 ± 10	35 ± 8	<5
Solar-size "β Hyi"	25	14	<2

NOTE.—The table shows measured *EXOSAT* soft X-ray fluxes from β Hyi and simulated observations of the Sun seen as a star at the distance of β Hyi. Photon counts per hour through different X-ray broad-band filters are given. The bottom line shows the flux from a star the size of the Sun with the activity level of β Hyi.

puted for metallicities equal to the "cosmic" abundance (Allen 1973), used here for the Sun, and one-half that value. When required, fluxes for the best estimate of the β Hyi metallicity, [Me/H] = −0.2 (Paper I), were obtained by an interpolation between these models. A halved metallicity has the effect of somewhat (by typically a factor 2) lowering the X-ray flux. Negligible interstellar absorption is assumed, as appropriate for nearby stars.

For a temperature of $T = 2 \times 10^6$ K, and "cosmic" abundances, these models produce an emissivity that rather closely reproduces observed solar fluxes for accepted values of the electron density, etc., of the solar corona.

3.3.1. *EXOSAT Filter Ratios*

A color temperature can be derived from the ratio of count rates in the Lexan and Al-Pa filters. The synthetic spectra were folded with the *EXOSAT* filter transmission curves, and the ratio between their respective count rates computed for coronae at different temperatures: Figure 4. The three bold curves show different filter ratios for a metallicity equal to one-half "cosmic" abundances, close to those of β Hyi. The observed aluminum-Parylene to 3000 Lexan ratio for β Hyi is marked, together with the observational error. For the Al-P to boron, and 3000 Lexan to boron ratios, the observational lower limits are the long-, and short-dashed lines. The solar Al-P/Lex ratio, computed from simulated *EXOSAT* observations, is the thin-dotted line, whose error bar marks the variability due to changes in solar activity. The solar data should be compared against the theoretical Al-P/Lex curve for "cosmic" abundances (dash-dotted). The distinctly different filter ratios of β Hyi and the Sun indicate a clear difference in coronal temperature. For β Hyi, the observations permit two solutions: either a "cool" (lukewarm) corona at log $T \simeq 5.7$ ($\simeq 5 \times 10^5$ K) or a hot one at log $T \simeq 6.6$ ($\simeq 4 \times 10^6$ K).

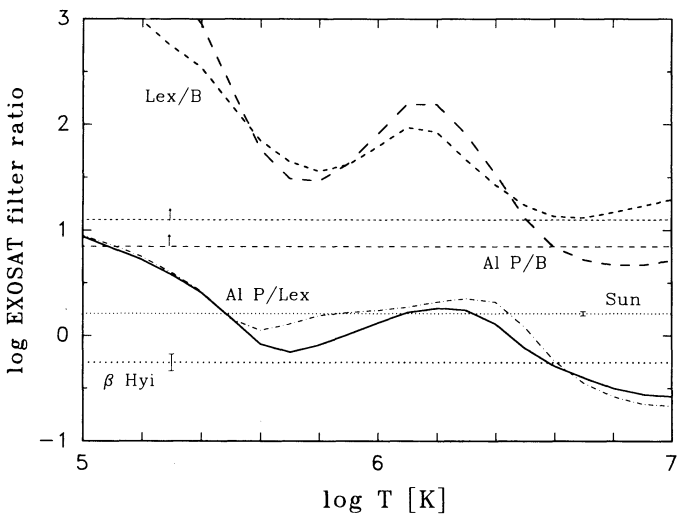

FIG. 4.—Ratios between count rates for pairs of *EXOSAT* filters, as function of plasma temperature. The bottom curves show Al-P to Lexan ratios: the bold-dotted line is the observed one for β Hyi, and the thin-dotted that of the Sun. The bold solid curve gives synthetic ratios for a plasma emissivity model with one-half "cosmic" abundances (as in β Hyi), while the dash-dotted curve is for "cosmic" abundances (as in the Sun). The upper curves show the Al-P to boron (*long-dashed*) and Lexan to boron (*short-dashed*) ratios for one-half "cosmic" abundance. The straight lines are the observational lower limits for β Hyi. The distinctly different filter ratios for β Hyi and the Sun indicate different temperatures. For β Hyi, two solutions are permitted: either a "cool" corona at log $T \simeq 5.7$, or a hot one at log $T \simeq 6.6$.

However, the complex shape of the filter transmission curves and that of the X-ray emissivity, combined with the observational errors, limits the accuracy of this procedure. A more precise method is to compute, for each filter, the emission measure versus temperature and to search for common solutions for different filters.

3.3.2. *Emission Measure Analysis*

Following Pallavicini et al. (1988), we begin by assuming that the corona is isothermal. For each filter we then construct the loci of emission measure versus temperature allowed by the observed count rates (including errors) and search for regions of common interception. This procedure allows us to determine the range of temperatures and emission measures which simultaneously satisfy the available data within the isothermal approximation.

Figure 5 shows the volume emission measures, $\int n_e^2\, dV$ (cm^{-3}) for an isothermal corona around β Hyi, computed from our observed fluxes through different *EXOSAT* filters, and using the plasma emissivity model by Landini & Monsignori-Fossi (1990) for the β Hyi metallicity [Me/H] = −0.2. Solid lines indicate the domain allowed by observational errors for the aluminum-Parylene filter, and dashed lines for the 3000 Lexan one. The dotted curve is the upper limit from the boron filter measurements. The error limits are set at ±0.1 dex, which is worse than *EXOSAT* counting statistics alone, but they also take some account of the likely systematic errors.

As in Figure 4, there are *two* permitted solutions: one around log $T = 5.7$ ($\simeq 5 \times 10^5$ K), and the other around log $T = 6.6$ ($\simeq 4 \times 10^6$ K). The upper limit from the boron filter is insufficient to exclude the high-temperature solution. For the "cool" solution, log emission measures around 49.1 cm^{-3} are found, and $\simeq$49.6 cm^{-3} for the "hot" solution. The emission measure is obtained from $n_e^2 V = r^2\, F_{obs}/F_{pla}$, where F_{obs} is the observed flux, and F_{pla} = computed plasma emission in photons cm^5 s^{-1}. The β Hyi distance $r = 6.54$ pc = 2.02×10^{19} cm.

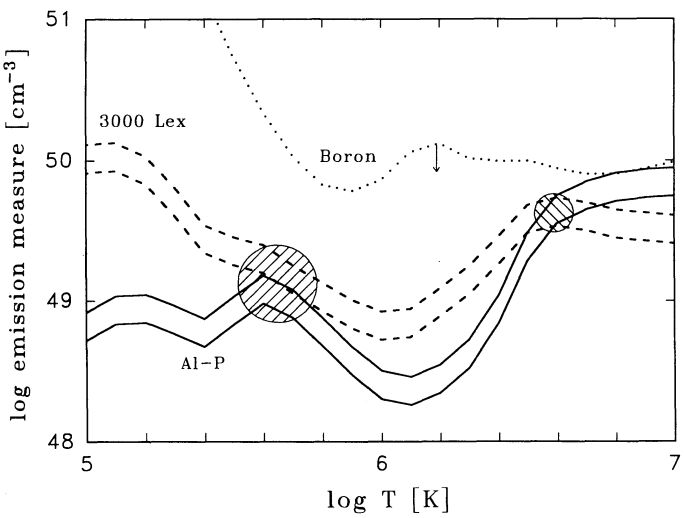

FIG. 5.—Volume emission measures for an isothermal corona around β Hyi, computed from *EXOSAT* fluxes, using the plasma emissivity model by Landini & Monsignori-Fossi. Solid lines indicate the domain allowed by observational errors for the aluminum-Parylene filter, and dashed lines for the 3000 Lexan one. As in Fig. 4, there are two permitted temperatures: either a "cool" corona around log $T = 5.7$, or a hot one at log $T = 6.6$.

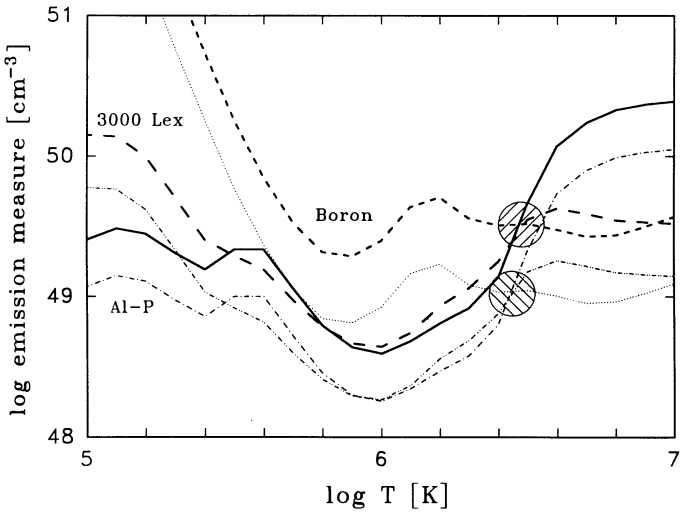

FIG. 6.—The X-ray Sun seen as a star. Emission measures are computed from simulated *EXOSAT* "observations." Bold (*solid, long-, and short-dashed*) curves show solar maximum conditions; for the aluminum-Parylene, 3000 Lexan, and the boron filters, respectively. Light curves (*dash-dotted, dash-double-dotted, and dotted*) show solar activity minimum.The model gives a well-defined solution for temperatures log $T \simeq 6.5$.

3.3.3. *The Sun Seen as a Star*

We now apply a similar technique to deduce properties of the solar corona from our *simulated EXOSAT* observations of the Sun seen as a star. The aim is, of course, not to gain new information about the Sun—there exist much superior data with high spatial, spectral, and temporal resolution—but rather to test to what extent the analysis methods presently available for stellar data give reasonably correct results, and especially to make a *differential* analysis of β Hyi versus the Sun.

Figure 6 shows volume emission measures for an assumed isothermal solar corona, as computed from the simulated "observations" (§ 3.2). The same plasma emissivity model as in Figure 5 is used, with metallicities equal to the "cosmic" abundances. Instead of the observed uncertainties in Figure 5, two curves for each filter show representative values for solar activity maximum (*bold*) and minimum (*light*). The model gives a (surprisingly?) well-defined solution for coronal temperatures log $T \simeq 6.5$ ($\simeq 3 \times 10^6$ K), with an average emission measure $\simeq 10^{49.3}$ cm^{-3}.

These deduced solar values can be compared against the commonly accepted ones, obtained from considerably more detailed data and models. The comparison is, however, made somewhat difficult by the circumstance that the solar corona is not only highly inhomogeneous, but also time-variable on almost all time scales. Already in *Skylab* data it was seen that it could change from maximum- to minimum-like configuration in a week or so. This physical variability adds another, possibly significant, source of uncertainty in the data compilations from which our solar data were taken.

The review by Golub (1983) concludes that, at solar maximum, the X-ray emission can be characterized by the properties of large active regions, with $T \simeq 10^{6.6}$ K, and an emission measure $\simeq 10^{50.5}$ cm^{-3}. At solar minimum, the corona is characterized by small emission regions with $T \simeq 10^{6.3}$ K and EM $\simeq 10^{49}$ cm^{-3}. Our values from Figure 6 fall well within this range, which seems encouraging in applying these rather simple models to stellar data.

3.3.4. *Deduced X-Ray Spectra*

As the next step, we now use the plasma emissivity models to compute synthetic spectra for coronae with parameters deduced from the emission measure analysis. These X-ray spectra from the "cool" solution for β Hyi, and for the Sun seen as a star, are shown in Figure 7. The β Hyi "cool" solution gave an emission measure $10^{49.1}$ cm^3 at log $T = 5.7$, and average solar conditions $10^{49.3}$ cm^3 at log $T = 6.5$ K. These latter values are also representative of the "hot" solution for β Hyi. The stellar flux in photons per second per energy interval is obtained by combining theoretical plasma emissivities with deduced emission measures.

From the deduced spectra in Figure 7, coronal energy fluxes can be computed for various energy ranges. The total flux for the "cool" β Hyi corona, within the *EXOSAT* 0.02–2.5 keV energy range is 4.5×10^{19} W (4.5×10^{26} ergs s^{-1}), but less than 1% of this value in the harder X-ray 0.2–4.5 keV range of *Einstein*—only 2.9×10^{17} W. The fluxes from the hotter solar corona are, however, quite comparable for the *EXOSAT* and *Einstein* ranges: 7.7×10^{19} and 3.7×10^{19} W, respectively.

We can compare these deduced solar values to commonly accepted values for its X-ray luminosity, keeping in mind the difficulties of detailed comparison due to solar variability and changing energy ranges in different instruments. In their review, Vaiana & Rosner (1978) give the average $L_x = 2 \times 10^{20}$ W (2×10^{27} ergs s^{-1}), ranging between 10^{20} and 10^{21} W. The weakest fluxes are observed in coronal holes, and a Sun entirely covered with such holes would have an X-ray luminosity $\simeq 5 \times 10^{19}$ W, one-tenth that of a Sun covered with quiet region structures. A Sun entirely covered with active regions would radiate $\simeq 2 \times 10^{22}$ W, if covered with small flares $\simeq 2 \times 10^{24}$ W, and another order of magnitude more if covered with bright flares.

3.3.5. *Uncertainties in the Coronal Modeling*

The derivation of coronal properties in β Hyi obviously contains uncertainties, both as regards the modeling of the X-ray emission, and the application of X-ray filter observations.

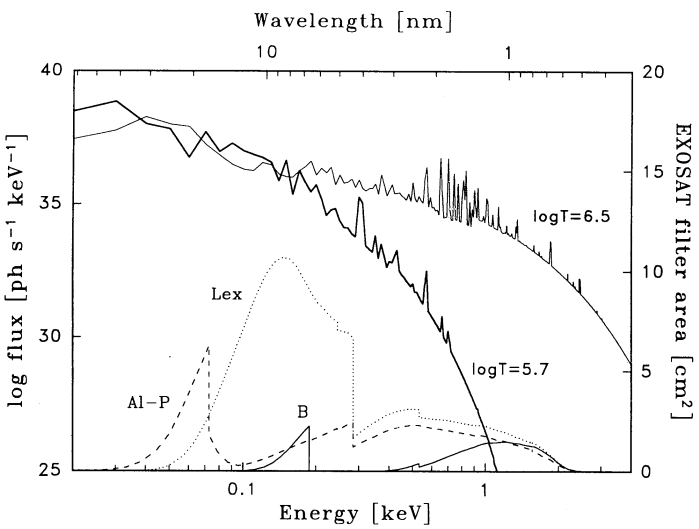

FIG. 7.—X-ray spectra of the "cool" solution for β Hyi (*bold*), and for the Sun seen as a star, as deduced from the emission measure analysis in Figs. 5–6. The "hot" solution for β Hyi is quite similar to the solar one. These spectra result from plasma emissivity models with the β Hyi metallicity [Me/H] = −0.2, and "cosmic" abundances for the Sun. At bottom, transmission profiles for *EXOSAT* filters are shown, with effective areas marked to the right.

The thermal X-ray spectrum is computed with a model of an optically thin plasma in collisional equilibrium. Although the problem of computing such a spectrum would appear to have a unique solution, in practice different models may give somewhat different results (e.g., Mewe, Gronenschild, & van den Oord 1985). Schmitt et al. (1985) analyze *Einstein* and *EXOSAT* data with the models of Raymond & Smith (1977) and Landini & Monsignori-Fossi (1984) and compare the results. Somewhat surprisingly, the derived temperatures from the two models agree to within the statistical errors, even for emission measures that vary by orders of magnitude.

If the source spectrum is produced by a distribution of emission measures, continuous with temperature, the coronal parameters derived adopting the usual fitting procedures may depend on the spectral response of the spectrometer used. For further discussions of the limitations generally present in X-ray filter spectroscopy, see Schmitt et al. (1987) and Pallavicini et al. (1988).

3.4. *Other Solar-Type Stars and Comparisons between EXOSAT, Einstein, and ROSAT Data*

The general lack of calibrated X-ray spectra makes it awkward to make precise comparisons between measurements from different instruments. Many analyses of stellar coronae are based upon observations from *Einstein*, to which we now compare our data. The fraction of the total X-ray flux contained in its IPC and HRI passbands depends on the coronal temperature, ranging from 15% at 10^6 K to 85% at $10^{6.8}$ K, as illustrated by Haisch & Simon (1982; their Table 3). The different sensitivities of *EXOSAT* and *Einstein* is illustrated by Schmitt & Rosso (1988; their Fig. 6) as function of plasma temperature.

Actually, an attempt was made to observe β Hyi from *Einstein*. The observing log shows it was observed 1979 September 19 with its solid state spectrometer for 10,000 s, but the data indicator shows absence of data, However, the efficiency of that instrument drops sharply below $\simeq 1$ keV, and β Hyi must have been too weak for detection. No observations with the imaging telescope appear to have been made.

Beta Hyi was recently observed as part of the all-sky X-ray survey from *ROSAT* and detected as a very soft source at energies less than 0.5 keV (J. H. M. M. Schmitt, private communication). However, any more detailed interpretation must await the availability of better spectral data.

3.4.1. *α Centauri A*

This slightly evolved solar "near-twin," α Cen A (G2 V), is an important comparison star for the Sun and β Hyi. Golub et al. (1982) found a volume emission measure of $2.0 \pm 0.2 \times 10^{49}$ cm^{-3}, and a luminosity $L_x = 1.2 \times 10^{20}$ W (1.2×10^{27} ergs s^{-1}), somewhat below the solar minimum value. Alpha Cen A is bolometrically more luminous, and hence larger than the Sun: $R_* = 1.23\ R_\odot$. With this radius, the stellar surface flux becomes 13 W m^{-2} (1.3×10^4 ergs cm^{-2} s^{-1}) versus 33 W m^{-2} for the typical quiet Sun.

3.4.2. *Other Stars with Evidence for a "Cool" Corona*

As discussed above, ambiguities in filter spectroscopy often preclude a unique determination of the coronal temperature. We now examine previous suggestions for "cool" coronae in other stars. Data for many stars observed with *Einstein* IPC were fitted to various models by Schmitt et al. (1990a). However, only in a few cases are there indications of temperatures below 10^6 K.

Procyon A (F5 IV–V) was one of the few stars for which *EXOSAT* obtained grating spectra, and Lemen et al. (1989) found the data consistent with a two-temperature corona of 0.5 and 2×10^6 K. If a one-temperature fit is forced on the data, the temperature becomes 0.6×10^6 K. Similar conclusions are in Schrijver (1985).

Schmitt et al. (1990a) fitted pulse height *Einstein* IPC data for Procyon, obtaining a one-temperature fit with $\log T = 6.2$, and another emission measure distribution fit with maximum temperature $\log T = 6.4$, the latter value being the coolest in their sample of more than 100 stars. A spectral analysis of stars in the Ursa Major stream was made from *Einstein* measurements by Schmitt et al. (1990b), who find one star (HD 39587, χ^1 Ori; G0 V) for which a two-temperature fit *possibly* indicates a component cooler than 10^6 K: $\log T_1 = 5.8$; $\log T_2 = 7.0$ K.

Pallavicini et al. (1988) compared *Einstein* and *EXOSAT* observations of coronae in late-type stars. Precise comparisons are awkward because the conversion factors between various filters depend on the generally unknown coronal temperature. There appears only one "anomalous" solar-type in the comparison: η Cas (G0 V + dM0), which was seen by *EXOSAT* at a level $\simeq 4$ times brighter than in previous *Einstein* IPC observations, assuming a standard conversion factor. One explanation could be that the M companion was flaring at the time of the *EXOSAT* measurements. Alternatively, η Cas could be a very soft source at $T \lesssim 10^6$.

Cool giants, such as Arcturus (K1 III) or α Ari (K2 III) were generally not detected by *Einstein* or *ROSAT*. However, Gondoin, Mangeney, & Praderie (1987) succeeded in detecting α Ari (K2 III) with *EXOSAT*. Its chromospheric radiative losses and X-ray flux are, respectively, one and two orders of magnitude lower than those of other F- and G-type giants observed, and no Si IV nor C IV emission is visible. The He I 1083 nm line further suggests the absence of strong coronal emission. The observed *EXOSAT* count rate can be explained by an emitting plasma of low temperature. The deduced surface flux for α Ari is $\simeq 0.3$ W m^{-2} (3×10^2 ergs cm^{-2} s^{-1}), much lower than the solar value at activity minimum. Such K giants may represent the stellar evolutionary state which β Hyi will reach after its present subgiant phase.

3.5. *Mechanisms for a "Cool" Corona*

If the "cool" coronal solution is correct, it probably implies that most of the heating mechanisms present in more active stars are missing from β Hyi, and that its coronal structure is possibly quite different from that of the Sun. We are not aware of any physical models for possible "cool" coronae in solar-type stars, but we want to point at some plausible processes that could be at work.

3.5.1. *The Stability of a "Cool" Corona*

The formation of coronae is the result of a complex balance between nonradiative energy input, and energy losses due to, e.g., radiation, downward heat conduction or cooling to a stellar wind. While any physical modeling of coronae has to treat all these processes, we will limit our comments to the thermal stability of plasmas. For a plasma to be stable against small thermal perturbations, the emissivity has to *increase* with increasing temperature, so that an increase of nonradiative heating causes a slightly higher temperature, which compensates by increased radiative losses.

Since the emissivity of a plasma is a somewhat complex

function of temperature, there is only a limited number of temperature intervals for thermal stability. An examination of the models for radiative emission from optically thin plasmas shows there to actually exist (marginally) stable regions also at cooler temperatures than the solar coronal one of $\simeq 2 \times 10^6$ K. For the models used in the present work, there is a (shallow) minimum in the radiative losses at log $T = 5.8$, going up to a maximum at log $T = 6.1$ K (Landini & Monsignori-Fossi 1990; their Fig. 9). In an analogous manner, Mewe et al. (1985; their Fig. 1) find the emissivity in the 0.1–25 nm band to have a minimum around log $T \simeq 5.7$, before a maximum at log $T \simeq 6.1$ K.

At temperatures around $\simeq 5 \times 10^5$ K, there is thus a (local) minimum of the radiative losses: the plasma emissivity is higher at either cooler or higher temperatures. A similar phenomenon occurs at 2–3 $\times 10^6$ K, and again around 20 $\times 10^6$ K. Lemen et al. (1989) analyzed *EXOSAT* grating spectra from three stars of widely different activity levels (including Procyon; § 3.4.2), finding evidence for these three temperature regions only. Also Schrijver, Dobson, & Radick (1992) find evidence for "cool" components at $\simeq 5 \times 10^5$ K.

3.5.2. *Processes in the Solar Corona*

Magnetically controlled loops appear to be a fundamental component of the solar corona. Virtually all of the emission originates in topologically closed, looplike structures, while regions with significant mass outflow ("coronal holes") contribute almost negligibly to the integrated X-ray emission. Within the relevant temperature ranges, the plasma emissivity changes only rather slowly with temperature, and the change in the coronal cooling rate can therefore only be a slowly varying function of temperature alone. This implies that the great variation in X-ray luminosity between solar maximum and minimum must largely be due to different amounts of coronal material present, even if there is a hardening of the solar X-ray spectrum with increased level of activity.

A number of reviews exist with more detailed discussions of solar coronal physics. Of particular relevance for X-ray observations, and for the solar-stellar connection are Vaiana & Rosner (1978), Golub (1983), Vaiana (1983), and Rosner, Golub, & Vaiana (1985).

3.5.3. *Acoustic Heating Mechanisms*

Various physical mechanisms likely to heat stellar chromospheres and coronae are surveyed by Narain & Ulmschneider (1990). These include various Alfvén and other magnetohydrodynamic waves, dissipation of electric currents and reconnection of magnetic fields, heating by microflares, and damping of acoustic waves. Irrespective of magnetic activity, acoustic waves from thermally driven motions in stellar photospheres provide a mechanism for heating outer atmospheric layers.

As discussed in Paper II, acoustic heating might be able to generate chromospheric emission features in solar-type stars, but corresponding acoustically heated coronal models have very low base pressures and energy fluxes. The energy available for X-ray emission is found to be some two to three orders of magnitude smaller than observed X-ray fluxes for the Sun (Stepień & Ulmschneider 1989; Hammer & Ulmschneider 1990). Accepting these results means that observable stellar coronae (including that of β Hyi) must predominantly be energized by magnetic heating mechanisms.

3.6. *The Coronal Dividing Line in the H-R Diagram*

Ayres et al. (1981a) called attention to the absence of X-ray emission from evolved single stars of spectral type K and cooler. An extensive survey based on *Einstein* data was compiled by Maggio et al. (1990). In observations of 380 giants of spectral types F to M, none of the M types was detected, 14% of the K, and 45% of the G. The drop in X-ray detections around K3 constitutes the X-ray "dividing line" in the Hertzsprung-Russell diagram. These results are reinforced by the statistics of the recent *ROSAT* all-sky X-ray survey (Haisch et al. 1991).

This coronal "dividing line" coincides with that for transition region indicators (Haisch et al. 1990). The absence (or paucity) of hot plasma in the cooler giants could be a result of their slow rotational velocities, which seem likely to weaken the generation and amplification of magnetic fields through the dynamo mechanism. However, there may be limits to how far the solar analogy can be pushed, since other processes may become important: e.g., this "dividing line" also largely coincides with that for the onset of strong stellar winds. Several authors have discussed possible mechanisms behind this "dividing line," but only very few physical theories have emerged.

With its low activity level (detectable only thanks to its proximity), β Hyi could be sufficiently close to the "dividing line" to illustrate some of the physical processes that are responsible for the decay of transition regions and coronae in evolved cooler stars. Although, at G2 IV, β Hyi is still some distance away from the dividing line proper, its evolutionary track is carrying it in that direction.

From a solar analogy, we can propose a scenario for β Hyi. As discussed in Paper II, the weak variability of chromospheric activity suggests the absence of any more significant active regions. Consequently, there might be only limited amounts of emerging magnetic flux, precluding the formation of closed magnetic loops in the corona. Without magnetic loops to confine and heat the coronal plasma in a solar-type manner, much of the surface of β Hyi would then have the appearance of solar-type coronal holes.

3.7. *Time Evolution of Stellar Coronae*

Coronal X-ray flux declines very rapidly with increasing stellar age, and clues to the fundamental mechanisms behind it might be obtained by studying stars of extreme activity levels, such as stars in very young clusters or very old stars such as β Hyi.

3.7.1. *Coronae in Stars of Different Age*

It is now possible to follow the time evolution of coronae in solar-type G stars over almost four decades in age. Of all spectral types, it is the solar-type stars which show the strongest evolution of X-ray luminosity with age and the most obvious dependence of L_x on rotation. A number of authors have studied stars of different age, in particular those belonging to young clusters. In Figure 8, we have compiled such data for near–main-sequence stars around spectral type G, comparing to present results for β Hyi.

The youngest G stars (still in their T Tauri phase) are found in young stellar associations. Smith, Pravdo, & Ku (1983) studied such objects in the Orion Ic cluster, whose age estimate is $\simeq 1$–4×10^6 yr. Pre–main-sequence stars in the Chamaelon dark cloud were observed by Feigelson & Kriss (1989), and "naked" T Tauri stars in the Taurus-Auriga complex by Walter et al. (1988). (The "nakedness" refers to the apparent lack of circumstellar material, and these appear to be basically normal stars with ages 1–40 $\times 10^6$ yr.)

The Pleiades cluster ($\simeq 10^{7.7}$ yr) has been an important target of investigation. The final analysis of the *Einstein Obser-*

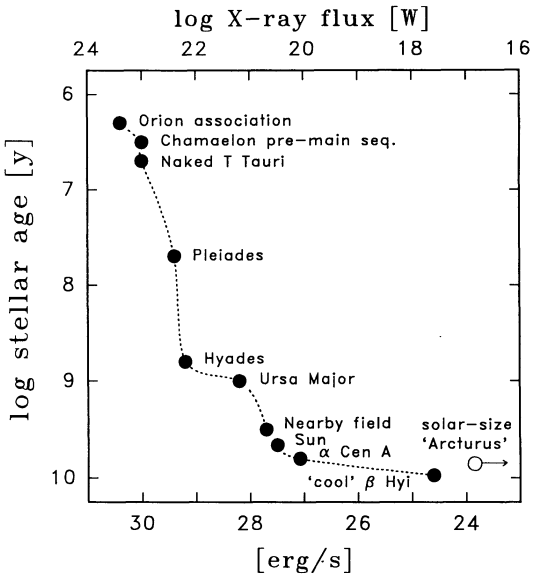

FIG. 8.—The decay of coronal X-ray flux with increasing age in solar-type stars. Observed *Einstein* fluxes are compiled from various sources and compared to present results for β Hyi within the same X-ray energy band. For β Hyi, its "cool" solution is shown (the "hot" one is comparable to the Sun and α Cen A). Coronal activity declines further for even more evolved stars, as shown by the *ROSAT* upper limit for the Arcturus activity level, scaled to a *solar-size* star.

vatory survey is by Micela et al. (1990), who detected 85 of 283 Pleiades stars in the surveyed region. The X-ray emission for the solar-like Pleiades stars is some two orders of magnitude more intense than that of the Sun. For the Hyades, the final *Einstein* survey is by Micela et al. (1988), detecting 66 out of 121 members.

X-rays from the Ursa Major cluster have been studied by Walter et al. (1984) and Schmitt et al. (1990b), who detected 18 out of 42 members surveyed. They were surprised to find a mean X-ray luminosity lower than in the Hyades, which are not significantly younger than the Ursa Major group. However, quite probably the star sample is contaminated by field stars.

Nearby solar-type stars in a volume-limited sample ($d < 25$ pc) were surveyed by Maggio et al. (1987); their typical age is probably $\simeq 3 \times 10^9$ yr. For the Sun, most authors use the value $10^{20.5}$ W, also adopted here. The α Cen A observation is from Golub et al. (1982). We also show a data point from the *ROSAT* upper limit for the *surface flux* of Arcturus (Ayres et al. 1991). This point in Figure 8 refers to the integrated flux for a *solar-size* star, illustrating that coronal X-ray activity continues to decline also in later stages of stellar evolution. (All other data points refer to solar-size stars, where there is a unique conversion between X-ray luminosity and surface flux.) The cluster data are from surveys made from *Einstein*, and thus are measures of the soft X-ray flux in its particular passband. For consistency, our points for β Hyi were computed for the 0.2–4 keV *Einstein* passband by integrating the deduced X-ray spectra in Figure 7. The "cool" solution for β Hyi is shown (the "hot" one is comparable to the Sun and α Cen A). In the former case, the particularly low flux value is mainly caused by the soft spectrum largely falling outside the *Einstein* passband.

As a caveat to Figure 8, we caution that published X-ray luminosities in stellar clusters must systematically be somewhat overestimated: the data points refer to the averages of *detected* stars, while a certain portion of the cluster members remain unseen. In particular, the different detection thresholds for differently distant clusters makes it awkward to make statements about the fainter stars, and of the full spread in X-ray luminosity among different cluster members.

3.7.2. *Functional Forms for the Age Dependence*

Several authors have attempted to identify analytical functions to describe the age decay of coronal X-ray flux, but we leave it to the reader to find functions to fit the data in Figure 8. Adopting the "cool" solution for β Hyi, we see a continued rapid decrease of L_x from solar-age stars to β Hyi. However, much of this decrease merely reflects the lower coronal temperature, which shifts much of the radiated flux outside that particular passband for soft X-rays which happened to be characteristic of the *Einstein* satellite, and which is used for Figure 8. This instrumental dependence would appear to put some doubts on the physical significance of the widespread fitting of analytical functions.

3.7.3. *The Dependence on Stellar Rotation*

Statistically, stellar rotation decreases with increasing age, and thus stellar activity is statistically lower in slow rotators. It is less obvious whether any of these parameters (age or rotation) is fundamental in controlling stellar activity. Several studies have been made for the relation between stellar X-ray flux and stellar rotation. For β Hyi, our determined value for $v \sin i$ of 2 ± 1 km s^{-1} (Paper I) implies a rotational period of $\simeq 45 \sin i$ days (with $R_* = 1.6\ R_\odot$). Although perhaps not much slower than solar rotation, this is an order of magnitude less than for most other solar-type stars with observed coronae which have reliable rotation data available.

3.8. *Other Coronal Indicators*

There are other indicators for stellar coronae besides X-rays. The Very Large Array radio telescope has been used to detect microwave flux from coronae in several classes of stars, but it cannot observe β Hyi at its southern declination of $-77°$. Stellar microwave detections have so far been limited to very active stars only, and a detection of β Hyi appears unlikely at the present time. However, with improved instrumental sensitivity, perhaps a try with the *Australia* radio telescope could become worthwhile sometime in the future?

Also, the He I 1083 nm line is sensitive to coronal activity and may be a good proxy for the soft X-ray flux (cf. Paper II). The population of the lower state of the He I transition in the Sun and late-type stars is probably determined by recombination following photoionization of He I X-rays shining down from a hot corona (Zirin 1975). However, this line has not yet been observed in β Hyi.

4. THE STELLAR WIND

As discussed above, the limited spectral information in the X-ray data leads to an ambiguity in the deduced coronal temperature (besides the additional uncertainties that may arise if the corona would be strongly inhomogeneous). The possibility of a "cool" corona is especially intriguing, because such a low temperature might be insufficient to drive a stellar wind of the solar type.

4.1. *Requirements for Wind Existence*

The physical mechanisms supposed to accelerate the solar wind are either the action of a thermal pressure gradient in the corona and/or the deposition of momentum flux carried by

Alfvén waves. The hydrodynamic expansion of the present solar corona requires a coronal base temperature in excess of $\simeq 0.7 \times 10^6$ K. If, during the future course of solar evolution, the energy input into the corona would decrease by only a rather modest factor, the present type of solar wind would cease to exist (unless some other acceleration mechanism takes over).

The minimum coronal temperature required to produce a solar wind expansion in a simple model is (e.g., Hundhausen 1972; § I.4):

$$T_{\min} = \frac{\alpha - 1}{2\alpha} \frac{G\mathfrak{M}_\odot\, m}{k r_0}, \qquad (1)$$

where G is the gravitational and k the Boltzmann constant, $\mathfrak{M}_\odot$ the solar and m the proton mass, and r_0 the radial distance to the base of the solar wind flow. The variation of temperature is assumed to follow a polytrope law with index α. For solar conditions $\alpha \simeq 1.1$, which leads to $T_{\min} \simeq 0.73 \times 10^6$ K.

If the coronal temperature would fall below this critical value, its hydrodynamic expansion would cease, and the corona would then be subject to a mere kinetic evaporation, analogous to the thermal escape of the outer parts of a planetary atmosphere.

A consequence of such a possible windless situation could be an effective cessation of the braking of the stellar rotation. The mechanism for losing stellar angular momentum through a magnetic stellar wind might be largely lost, and without this mechanism (operational since the formation of the star) there would be little further changes of stellar rotation and (assuming that activity is controlled by rotation), no significant further secular changes of chromospheric and coronal activity, at least not until the star begins its evolution into a red giant.

As discussed in § 2.7, there is indeed evidence that cool subgiants undergo no further major changes in their activity, after leaving their main-sequence life and before their red giant stage (Simon & Drake 1989). This result seems consistent with such a cessation of magnetic braking mechanisms.

4.2. *Loss of Solar Wind in the Past?*

It is not inconceivable that the temperature of the *solar* corona could fall below the critical value during periods of very low activity, such as the Maunder minimum in the late 17th century (which might have analogies with the present β Hyi). To determine whether the solar wind actually ceased during these periods appears quite difficult, though perhaps not impossible. It would appear that, in the absence of a solar wind, comets could not develop the (often bluish) *ion* tail in addition to their ordinary (yellowish) *dust* one, something which careful observers could well have noticed.

Systematic catalogs of comet observations throughout the ages have been compiled by a few authors. Vsekhsvyatskii (1964) lists comet sightings from the year 466 B.C. onward. There are 10 reports during the 15th century, 14 in the 16th, 21 in the 17th, and 63 in the 18th century. Of these, 21 comets appeared between 1652 and 1707, during the Maunder minimum. However, comments on the color of the tail are given only in two cases: the tail of the 1668 comet was "brilliant white," and the 1686 one was "equal in color to [the A4-type star] δ Leo." Later and earlier comets occasionally have their colors noted: The one in 1744 had "a reddish-yellow tail;" the 1786 II a "color comparable to [the Dumbbell planetary nebula] M27," and the 1593 "matched [the A7-type star] α Cep in color." The 1556 comet had a "reddish head, with a straw-colored tail," the 1506 and 1468 ones were "bluish," the 1362 had an "ash-colored tail," the 1337 comet was noted for its "whiteness," while the 989 A.D. apparition of comet Halley looked "bluish-white."

Although this discussion is insufficient to judge whether the solar wind was absent during some periods in the past, it does suggest that a systematic analysis of ancient records could reveal some systematic changes in the observed properties of comets and might permit more definitive conclusions.

Compared to the Sun, the coronal base height r_0 for β Hydri will presumably be larger (reflecting the larger stellar radius), and the temperature requirements for stellar wind expansion thus slightly lower. It does not appear feasible at present to examine more detailed questions about the stellar wind structure in β Hyi, but for the future, detailed X-ray spectroscopy (Mewe 1991) should be used to better diagnose the coronal and stellar wind conditions.

5. OUTLOOK FOR FUTURE CASE STUDIES

With the present Papers I–III, we have now concluded a systematic survey of the properties of β Hyi, starting with its global stellar attributes, and then moving up through its successive atmospheric layers. In the process, we have learned to know β Hydri as a star with a certain "personality." Besides for its specific results, this survey should demonstrate how a *case study* of an individual star, done in contrast to another well-known case (here the Sun), can illuminate stellar properties in a manner not readily possible with only statistical data from many "anonymous" stars. A logical next step could be to carry out a case study for the even more distant future of solar activity: to scrutinize a solar-mass star still more evolved than β Hyi, one which already has evolved well toward the red giant branch.

The Swedish part of this project was supported by the Swedish National Space Board and by the Swedish Natural Science Research Council. The development of *IUE* data analysis methods in Lund received support also from the European Space Agency. At Lund, H. Gleisner, H. Jakobsson, and U. Torkelsson contributed to parts of the analysis. We thank J. H. M. M. Schmitt (Garching) for communicating *ROSAT* results in advance of publication. H. Rickman (Uppsala) advised on literature for comet observations from past centuries, and an anonymous referee helped to clarify a number of points. J. L. Linsky acknowledges NASA grant NAG5-82 to the University of Colorado.

REFERENCES

Allen, C. W. 1973, Astrophysical Quantities (3d ed.; London: Athlone)
Ayres, T. R., Fleming, T. A., & Schmitt, J. H. M. M. 1991, ApJ, 376, L45
Ayres, T. R., Judge, P., Jordan, C., Brown, A., & Linsky, J. L. 1986, ApJ, 311, 947
Ayres, T. R., & Linsky, J. L. 1980, ApJ, 235, 76
Ayres, T. R., Linsky, J. L., Margon, B., & Bowyer, S. 1978, A&A, 70, 431
Ayres, T. R., Linsky, J. L., Vaiana, G. S., Golub, L., & Rosner, R. 1981a, ApJ, 250, 293
Ayres, T. R., Marstad, N. C., & Linsky, J. L. 1981b, ApJ, 247, 545
Ayres, T. R., Simon, T., & Linsky, J. L. 1982, ApJ, 263, 791
Bennett, J. O. 1987, Ph.D. thesis, University of Colorado, Boulder
Bohlin, R. C., Harris, A. W., Holm, A. V., & Gry, C. 1990 ApJS, 73, 413

Böhm-Vitense, E., & Woods, J. 1983, ApJ, 265, 331
Bonnet, R. M., Bruner, E. C., Acton, L. W., Brown, W. A., & Decaudin, M. 1980, ApJ, 237, L47
Brown, A., Jordan, C., Stencel, R. E., Linsky, J. L., & Ayres, T. R. 1984, ApJ, 283, 731
Cappelli, A., Cerruti-Sola, M., Cheng, C. C., & Pallavicini, R. 1989, A&A, 213, 226
Davelaar, J., & Giommi, P. 1985, EXOSAT Express, 10, 45
de Korte, P. A. J., et al. 1981, Space Sci. Rev., 30, 495
Dravins, D., Linde, P., Fredga, K., & Gahm, G. F. 1993b, ApJ, 403, 396 (Paper II)
Dravins, D., Lindegren, L., Nordlund, Å., & VandenBerg, D. A. 1993a, ApJ, 403, 385 (Paper I)
Feigelson, E. D., & Kriss, G. A. 1989, ApJ, 338, 262
Fontenla, J. M., Avrett, E. H., & Loeser, R. 1990, ApJ, 355, 700
Golub, L. 1983, in IAU Symp. 102, Solar and Stellar Magnetic Fields: Origins and Coronal Effects, ed. J. O. Stenflo (Dordrecht: Reidel), 345
Golub, L., Harnden, F. R., Pallavicini, R., Rosner, R., & Vaiana, G. S. 1982, ApJ, 253, 242
Gondoin, P., Mangeney, A., & Praderie, F. 1987, A&A, 174, 187
Gottwald, M. 1985, *EXOSAT* Express, 12, 67
Haisch, B. M., & Basri, G. 1985, ApJS, 58, 179
Haisch, B. M., Bookbinder, J. A., Maggio, A., Vaiana, G. S., & Bennett, J. O. 1990, ApJ, 361, 570
Haisch, B. M., Schmitt, J. H. M. M., & Rosso, C. 1991, ApJ, 383, L15
Haisch, B. M., & Simon, T. 1982, ApJ, 263, 252
Hammer, R., & Ulmschneider, P. 1990, in Cool Stars, Stellar Systems, and the Sun, ed. G. Wallerstein (ASPC 9), 51
Hundhausen, A. J. 1972, Coronal Expansion and Solar Wind (Berlin: Springer)
Jordan, C. 1991, in Mechanisms of Chromospheric and Coronal Heating, ed. P. Ulmschneider, E. R. Priest, & R. Rosner (Berlin: Springer), 300
Jordan, C., Ayres, T. R., Brown, A., Linsky, J. L., & Simon, T. 1987, MNRAS, 225, 903
Kinney, A. L., Bohlin, R. C., & Neill, J. D. 1991, PASP, 103, 694
Kreplin, R. W., Dere, K. P., Horan, D. M., & Meekins, J. F. 1977, in The Solar Output and its Variation ed. O. R. White (Boulder: Colorado Associated Univ. Press), 287
Landini, M., Monsignori-Fossi, B. C. 1984, Physica Scripta, T7, 53
———. 1990, A&AS, 82, 229
Landsman, W. B., Murthy, J., Henry, R. C., Moos, H. W., Linsky, J. L., & Russell, J. L. 1986, ApJ, 303, 791
Landsman, W., & Simon, T. 1991, ApJ, 366, L79
———. 1993, in preparation
Lean, J. 1987, J. Geophys. Res., 92, 839
Lemen, J. R., Mewe, R., Schrijver, C. J., & Fludra, A. 1989, ApJ, 341, 474
Maggio, A., Sciortino, S., Vaiana, G. S., Majer, P., Bookbinder, J., Golub, L., Harnden, F. R., & Rosner, R. 1987, ApJ, 315, 687
Maggio, A., Vaiana, G. S., Haisch, B. M., Stern, R. A., Bookbinder, J., Harnden, F. R., & Rosner, R. 1990, ApJ, 348, 253
Manson, J. E. 1977, in The Solar Output and its Variation, ed. O. R. White, (Boulder: Colorado Associated Univ. Press), 261
Mewe, R. 1991, A&A Rev., 3, 127
Mewe, R., Gronenschild, E. H. B. M., & van den Oord, G. H. J. 1985, A&AS, 62, 197
Micela, G., Sciortino, S., Vaiana, G. S., Harnden, F. R., Rosner, R., & Schmitt, J. H. M. M. 1990, ApJ, 348, 557
Micela, G., Sciortino, S., Vaiana, G. S., Schmitt, J. H. M. M., Stern, R. A., Harnden, F. R., & Rosner, R. 1988, ApJ, 325, 798
Narain, U., & Ulmschneider, P. 1990, Space Sci. Rev., 54, 377
Oranje, B. J. 1986, A&A, 154, 185
Paerels, F. B. S., Brinkman, A. C., den Boggende, A. J. F., de Korte, P. A. J., & Dijkstra, J. 1990, A&AS, 85, 1021
Pallavicini, R. 1989, A&A Rev., 1, 177
Pallavicini, R., Monsignori-Fossi, B. C., Landini, M., & Schmitt, J. H. M. M. 1988, A&A, 191, 109
Raymond, J. C., & Smith, B. W. 1977, ApJS, 35, 419
Rosner, R., An, C. H., Musielak, Z. E., Moore, R. L., & Suess, S. T. 1991, ApJ, 372, L91
Rosner, R., Golub, L., & Vaiana, G. S. 1985, ARA&A, 23, 413
Schmitt, J. H. M. M., Collura, A., Sciortino, S., Vaiana, G. S., Harnden, F. R., & Rosner, R. 1990a, ApJ, 365, 704
Schmitt, J. H. M. M., Harnden, F. R., Peres, G., Rosner, R., & Serio, S. 1985, ApJ, 288, 751
Schmitt, J. H. M. M., Micela, G., Sciortino, S., Vaiana, G. S., Harnden, F. R., & Rosner, R. 1990b, ApJ, 351, 492
Schmitt, J. H. M. M., Pallavicini, R., Monsignori-Fossi, B. C., & Harnden, F. R. 1987, A&A, 179, 193
Schmitt, J. H. M. M., & Rosso, C. 1988, A&A, 191, 99
Schrijver, C. J. 1985, Space Sci. Rev., 40, 3
Schrijver, C. J., Dobson, A. K., & Radick, R. R. 1992, A&A, 258, 432
Simon, T., & Drake, S. A. 1989, ApJ, 346, 303
Simon, T., Herbig, G., & Boesgaard, A. M. 1985, ApJ, 293, 551
Skumanich, A., & Lites, B. W. 1986, ApJ, 310, 419
Smith, M. A., Pravdo, S. H., & Ku, W. H. M. 1983, ApJ, 272, 163
Stepień, K., & Ulmschneider, P. 1989, A&A, 216, 139
Taylor, B. 1985, Adv. Space Res., 5, No. 3, 35
Timothy, J. G. 1977, in The Solar Output and its Variation, ed. O. R. White, (Boulder: Colorado Associated Univ. Press), 237
Vaiana, G. S. 1983, in IAU Symp. 102, Solar and Stellar Magnetic Fields: Origins and Coronal Effects, ed. J. O. Stenflo (Dordrecht: Reidel), 165
Vaiana, G. S., & Rosner, R. 1978, ARA&A, 16, 393
Vsekhsvyatskii, S. K. 1964, Physical Characteristics of Comets (Jerusalem: Israel Program for Scientific Translations)
Walter, F. M., Brown, A., Mathieu, R. D., Myers, P. C., & Vrba, F. J. 1988, AJ, 96, 297
Walter, F. M., Linsky, J. L., Simon, T., Golub, L., & Vaiana, G. S. 1984, ApJ, 281, 815
Zirin, H. 1975, ApJ, 199, L63